DOI: 10.1002/chem.201502052

Conducting Materials

$Li_{17}Sb_{13}S_{28}$: A New Lithium Ion Conductor and addition to the Phase Diagram Li_2S–Sb_2S_3

Sebastian Huber and Arno Pfitzner*[a]

Dedicated to Professor Manfred Scheer on the occasion of his 60th birthday

Abstract: $Li_{17}Sb_{13}S_{28}$ was synthesized by solid-state reaction of stoichiometric amounts of anhydrous Li_2S and Sb_2S_3. The crystal structure of $Li_{17}Sb_{13}S_{28}$ was determined from dark-red single crystals at room temperature. The title compound crystallizes in the monoclinic space group *C2/m* (no. 12) with $a = 12.765(2)$ Å, $b = 11.6195(8)$ Å, $c = 9.2564(9)$ Å, $\beta = 119.665(6)^\circ$, $V = 1193.0(2)$ Å^3, and $Z = 4$ (data at 20 °C, lattice constants from powder diffraction). The crystal structure contains one cation site with a mixed occupation by Li and Sb, and one with an antimony split position. Antimony and sulfur form slightly distorted tetragonal bipyramidal [SbS_5E] units (E = free electron pair). Six of these units are arranged around a vacancy in the anion substructure. The lone electron pairs E of the antimony(III) cations are arranged around these vacancies. Thus, a variant of the rock salt structure type with ordered vacancies in the anionic substructure results. Impedance spectroscopic measurements of $Li_{17}Sb_{13}S_{28}$ show a specific conductivity of $2.9\times10^{-9}\ \Omega^{-1}\,cm^{-1}$ at 323 K and of $7.9\times10^{-6}\ \Omega^{-1}\,cm^{-1}$ at 563 K, the corresponding activation energy is $E_A = 0.4$ eV below 403 K and $E_A = 0.6$ eV above. Raman spectra are dominated by the Sb–S stretching modes of the [SbS_5] units at 315 and 341 cm^{-1} at room temperature. Differential thermal analysis (DTA) measurements of $Li_{17}Sb_{13}S_{28}$ indicate peritectic melting at 854 K.

Introduction

The phase diagram Li_2S–Sb_2S_3 has been reported several years ago. Olivier-Fourcade et al. proposed several compounds therein, for example, $Li_{3x}Sb_{6-x}S_9$ ($x = 0.1$–0.5), $LiSbS_2$ (α, β, γ), $Li_6Sb_4S_9$, and Li_3SbS_3.[1,2] Only the rock salt type high-temperature modification of $LiSbS_2$ was characterized in detail at that time. However, these phase diagrams are quite helpful when searching for new ionic conductors.[3] The ionic conductivity has recently been characterized for the glassy systems of Li_2S–Sb_2S_3 combined with P_2S_5 and LiI or Li_3PO_4 by *Nagamedianova*.[4–6] In the course of investigations on new crystalline materials in the binary system Li_2S–Sb_2S_3 $LiSbS_2$-*mC*16 (hitherto unknown α-$LiSbS_2$) and Li_3SbS_3 were recently characterized by X-ray diffraction.[7,8] Li_3SbS_3 was also characterized by impedance spectroscopy, which revealed good ionic conductivity ($\sigma = 5.4\times10^{-5}\ \Omega^{-1}\,cm^{-1}$ at 573 K).[8] Besides this new ternary lithium compound, the corresponding sodium (Na_3SbS_3[9,10] and Na_3SbSe_3[11]), potassium (K_3SbSe_3[10]), rubidium (Rb_3SbSe_3[12]), cesium (Cs_3SbSe_3[12]), copper (Cu_3SbS_3[13–16] and Cu_3SbSe_3[17]), and silver (Ag_3SbS_3[18]) based materials of the same formula type are well-known and still of great interest. The sodium compounds show a good ion conductivity of $\sigma = 2\times10^{-6}\ \Omega^{-1}\,cm^{-1}$ at 570 K (Na_3SbS_3[9]) or $\sigma = 3\times10^{-6}\ \Omega^{-1}\,cm^{-1}$ at 590 K (Na_3SbSe_3[11]). The copper compounds are interesting thermoelectric materials[19,20] and exhibit a remarkably high diffusion coefficient of copper ions,[21] and Ag_3SbS_3 is a piezoelectric silver ion conductor.[22,23] Even mixtures of the ternary compounds with halides, for example, $(AgI)_2Ag_3SbS_3$ or $(CuI)_2Cu_3SbS_3$ show pronounced ionic conductivities.[24–27]

Another interesting point to note for compounds containing Sb^{3+} cations is the steric influence of their $5s^2$ lone pair of electrons (E). It has a significant structural influence, because of its pronounced steric requirements, and can cause strong structural or physical effects. The influence of lone electron pairs on physical properties like ferroelectricity, superconductivity, or semiconductivity is still an open question.[28,29] The cation eccentricity is a helpful measure of the lone pair activity.[30] Thus, the eccentricity of the cation positions for example in Sb_2S_3 or Bi_2S_3 is explained by this activity of the lone electron pair.[30,31] Distorted trigonal bipyramids [SbO_4E] and distorted tetrahedra [SbO_3E] are frequently observed.[32–34] Distorted tetragonal bipyramids [SbS_5E] are also known, for instance, in β-$LiSbS_2$ or $CuSbS_2$.[2,35] A model has been proposed for oxides where the lone electron pair has the same volume as an oxygen atom and thus can be considered as an atom of the coordination polyhedron.[36] The title compound is a further example of compounds containing [SbS_5E] distorted tetragonal bipyramids where the influence of the lone pairs on the crystal structure becomes quite obvious.

$Li_{17}Sb_{13}S_{28}$ is a new compound in the binary system Li_2S–Sb_2S_3 and shows an ordered arrangement of lone pairs of electrons of Sb^{3+} around vacancies in the anion lattice. Herein we

[a] Dr. S. Huber, Prof. Dr. A. Pfitzner
Institut für Anorganische Chemie
Universität Regensburg
Universitätsstrasse 31, 93040 Regensburg (Germany)
E-mail: arno.pfitzner@chemie.uni-regensburg.de

report on the synthesis, the structural characterization, and physical properties of $Li_{17}Sb_{13}S_{28}$.

Results and Discussion

Structure description and discussion

The crystal structure of $Li_{17}Sb_{13}S_{28}$ was determined by single-crystal X-ray diffraction. Crystallographic data are summarized in Table 1, atomic coordinates and isotropic displacement parameters in Table 2. $Li_{17}Sb_{13}S_{28}$ crystallizes in the monoclinic space group *C*2/*m* (no. 12). The structure consists of two Sb sites (one site has a split position), five S sites, three Li sites, and one site with a mixed occupation by Li and Sb. The Sb content on the mixed Li/Sb site is 25%. Li(1) and Li(2) have an octahedral environment [LiS_6] with *d*(Li–S) = 2.60–2.81 Å, whereas Li(3) has a 4 + 2 coordination with sulfur with four short bonds (*d*(Li–S) = 2.56–2.58 Å) and two longer bonds *d*(Li–S) = 3.03 Å. The shorter interatomic distances are in good accord with the sum of the Shannon radii, which is 2.60 Å, and with other compounds with an octahedral environment of lithium by sulfur.[48] The octahedra [LiS_6] are edge sharing. The mixed Li/Sb site has a 5 + 1 coordination with *d*(Li/Sb–S) = 2.57–2.81 Å and 3.03 Å. The dominant structural feature of the title compound is a tetragonal bipyramidal [SbS_5E] unit. *E* represents the $5s^2$ lone electron pair of Sb^{3+}, which is supposed to be sterically active. Sb(1) is 3 + 2 coordinated by sulfur (*d*(Sb–S) = 2.40–2.47 Å and 3.18 Å), whereas Sb(2) shows a split position (*d*(Sb21–Sb22) = 0.36 Å) with a 3 + 2 coordination (*d*(Sb–S) = 2.40–2.63 Å and 2.91 Å). Such so-called secondary bonds are also known for other thiometalate compounds, for example, $MnSb_2S_4$,[37] Li_3SbS_3,[8] or Na_3SbQ_3 (*Q* = S, Se).[9,11] A survey of the length distribution of secondary bonds in thioantimonates(III) shows a preferences for such distances in the range from 2.9 and 3.25 Å.[49] Six of the [SbS_5E] units are connected by sharing four basal corners and are arranged around one vacancy in the anion lattice, see Figure 1.

Table 1. Crystallographic data for the structure analysis of $Li_{17}Sb_{13}S_{28}$.[a]

Compound	$Li_{2.125}Sb_{1.625}S_{3.5}$
formula weight [g mol^{-1}]	324.80
color	dark-red
crystal system	monoclinic
space group	*C*2/*m* (no. 12)
lattice constants [Å]	*a* = 12.765(2)
from powder diffraction	*b* = 11.6195(8)
	c = 9.2564(9)
	β = 119.665(6)°
cell volume [Å^{-3}], *Z*	1193.0(2), 8
ρ_{calcd} [g cm^{-3}]	3.646
diffractometer	Agilent SuperNova
$Mo_{K\alpha}$	λ = 0.71073 Å
absorption correction	multi-scan[42]
T [K]	123
2Θ range [°]	$6.6 \le 2\Theta \le 60.7$
Hkl range	$-17 \le h \le 17$
	$-15 \le k \le 15$
	$-12 \le l \le 9$
No. of reflections, R_{int}	5328, 0.0428
no. of independent reflections	1714
no. of parameters	76
program	SHELX-2014[47]
final *R*/*wR* ($I > 2\sigma_I$)	0.0364, 0.0866
final *R*/*wR* (all reflections)	0.0432, 0.0928
GooF	1.052
largest difference peak $\Delta\rho_{max}$	1.26
and hole $\Delta\rho_{min}$ [e Å^{-3}]	−1.56
extinction coefficient	0.0016(1)

[a] Further details on the crystal structure investigations may be obtained from the Fachinformationszentrum Karlsruhe, 76344 Eggenstein-Leopoldshafen, Germany (Fax: (+49) 7247-808-666; E-mail: crysdata@fiz-karlsruhe.de), on quoting the depository number CSD-429902.

Table 2. Atomic coordinates and equivalent isotropic displacement parameters U_{eq}[a] for $Li_{17}Sb_{13}S_{28}$.

Atom	Wyck.	Occ.	*x*	*y*	*z*	U_{eq}
Sb1	4*i*	1.0	0.69500(4)	0	0.31769(6)	0.0182(2)
Sb21	8*j*	0.655(7)	0.39918(8)	0.1579(1)	0.1071(1)	0.0193(3)
Sb22	8*j*	0.345(7)	0.4116(2)	0.1810(2)	0.0950(2)	0.0190(4)
Sb3/ Li4	4*i*	0.25 0.75	0.8928(1)	0	0.0817(2)	0.0191(3)
S1	4*i*	1.0	0.8812(1)	0	0.5771(2)	0.0184(3)
S2	4*g*	1.0	0	0.1544(1)	0	0.0250(4)
S3	8*j*	1.0	0.3233(1)	0.3114(1)	0.2070(2)	0.0294(3)
S4	8*j*	1.0	0.60160(9)	0.15952(9)	0.3926(1)	0.0197(3)
S5	4*i*	1.0	0.3025(2)	0	0.2021(2)	0.0259(4)
Li1	2*d*	1.0	0.5	0	0.5	0.027(4)
Li2	8*j*	1.0	0.1902(8)	0.1613(7)	0.294(1)	0.028(2)
Li3	4*h*	1.0	0	0.142(1)	0.5	0.028(3)

[a] U_{eq} is defined as one third of the trace of the orthogonalized U_{ij} tensor.

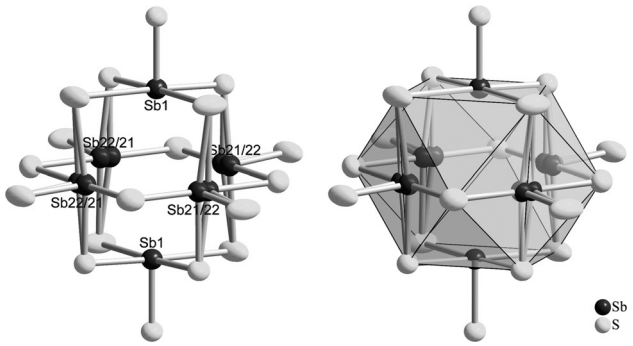

Figure 1. Cuboctahedral environment of six [SbS_5E] units arranged around a vacancy in the anion lattice.

The sulfur atoms build a cuboctahedral environment around the vacancy. The Sb^{3+} $5s^2$ lone pairs of electrons are all pointing to the center of the vacancy. The shortest Sb–Sb distance is *d*(Sb–Sb) = 3.47 Å, the shortest distance of opposite Sb atoms is *d*(Sb–Sb) = 5.40 Å. Comparable results can be found in β-$LiSbS_2$ (3.73 and 5.39 Å), which contains the same building units.[2] Overall there are two vacancies per unit cell. They are located on eight edges of the cell at 0, 0.5, 0, and 0.5, 0, 0. The cuboctahedron and the octahedron around the mixed Li/Sb

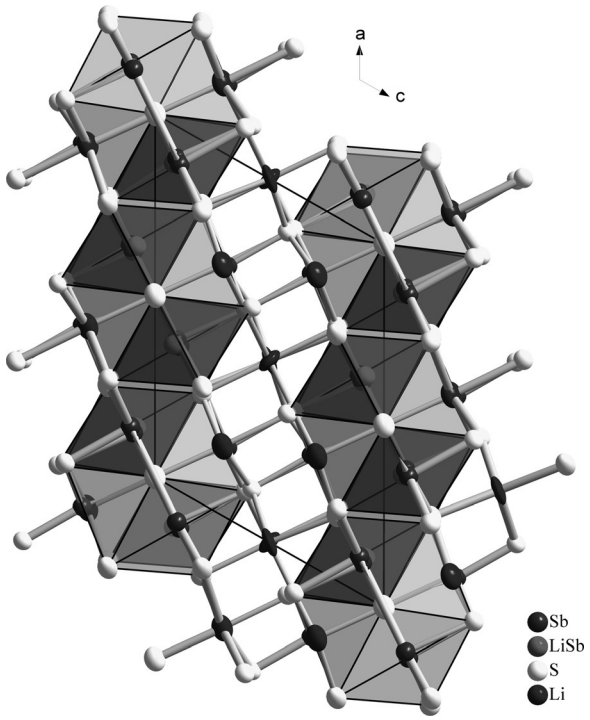

Figure 2. Layers of the cuboctahedra (light-gray) and the octahedral around the mixed Li/Sb position (dark-gray) parallel (001).

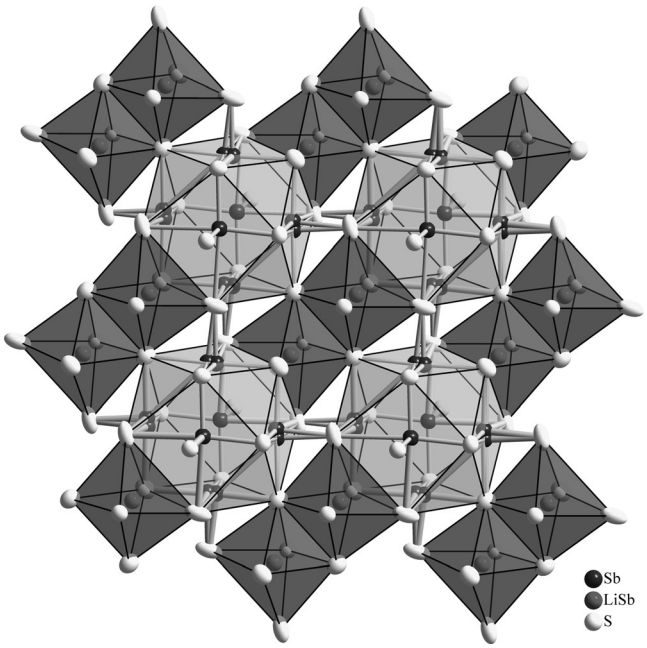

Figure 3. Connection of the cuboctahedra and the octahedra coordinating the mixed Li/Sb positions. Lithium atoms are omitted for clarity.

position are connected by sharing one face and one corner and are arranged in layers parallel to (001) (Figures 2 and 3).

Powder X-ray diffraction

The measured diffraction pattern of $Li_{17}Sb_{13}S_{28}$ shows that the sample obtained from the solid-state reaction is phase pure. A comparison with the pattern calculated from single-crystal structure data is shown in Figure 4. For a better comparability the room-temperature lattice constants from powder diffraction were used for the calculation.

In 1983 Olivier-Fourcade et al. published a compound with the composition $Li_6Sb_4S_9$ without any information on structural data.[1,2] $Li_{17}Sb_{13}S_{28}$ (= $Li_{5.46}Sb_{4.18}S_9$) has almost the same composition as $Li_6Sb_4S_9$. The powder patterns of $Li_{17}Sb_{13}S_{28}$ and "$Li_6Sb_4S_9$" match quite well (Figure 5), that is, "$Li_6Sb_4S_9$" reported in ref. [1] is supposed to be equivalent to $Li_{17}Sb_{13}S_{28}$.

Impedance spectroscopy

Cold pressed samples of $Li_{17}Sb_{13}S_{28}$ were used for impedance spectroscopic measurements. The samples were pressed for this purpose with 6000 kg cm^{-2} to pellets and connected with gold as ion blocking electrode material. Nyquist plots show semicircles at high frequencies and Warburg impedance arcs at low frequencies. For temperatures below 403 K the Warburg impedance arc is poorly resolved. Specific ionic conductivities increase upon heating from $2.9\times10^{-9}\,\Omega^{-1}\,cm^{-1}$ at 322 K to $8.0\times10^{-6}\,\Omega^{-1}\,cm^{-1}$ at 564 K. The corresponding Arrhenius type diagram provides an activation energy of $E_A = 0.4$ eV below 403 K and of $E_A = 0.6$ eV above. Figure 6 shows the ionic conductivity as a function of temperature.

The corresponding admittance spectra show the conductivity data for different temperatures. Therefore log G (conductance) data were plotted versus log f (frequency) for each temperature (see Figure 7). At low temperatures (323 K) a conductance dispersion can be observed at frequencies above 50 Hz, which is due to the occurrence of migration losses.[38] This loss of migration explains the poorly resolved Warburg impedance arcs in Nyquist plots below 403 K. The equivalent circuit for fit-

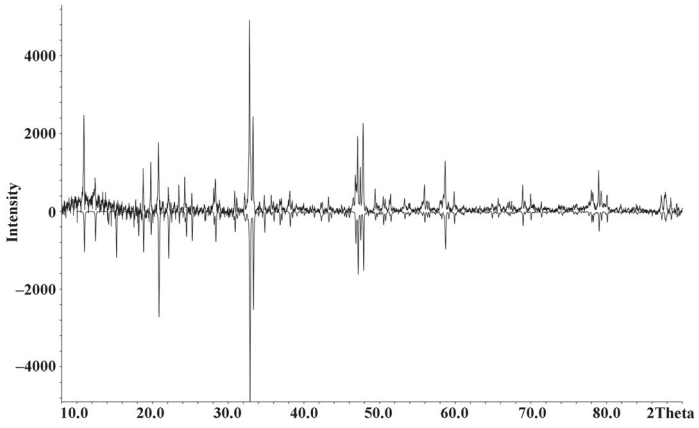

Figure 4. Comparison of measured (top, background corrected) and calculated X-ray powder diffraction pattern for $Li_{17}Sb_{13}S_{28}$ (bottom, negative intensities, lattice constant from powder diffraction).

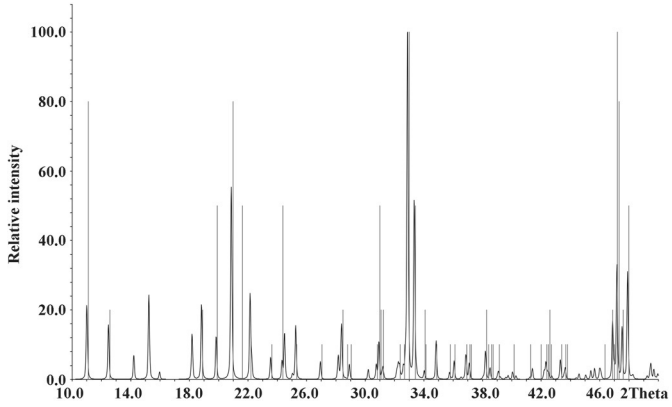

Figure 5. Comparison of a calculated X-ray powder diffraction pattern for $Li_{17}Sb_{13}S_{28}$ (black) and literature data for "$Li_6Sb_4S_9$" (gray vertical lines).

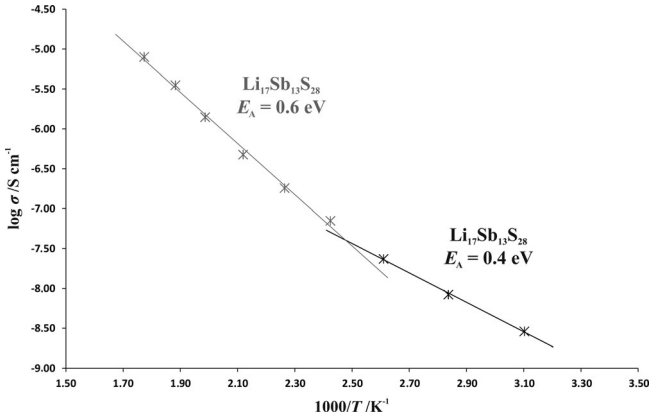

Figure 6. Temperature dependence of the ionic conductivity of $Li_{17}Sb_{13}S_{28}$.

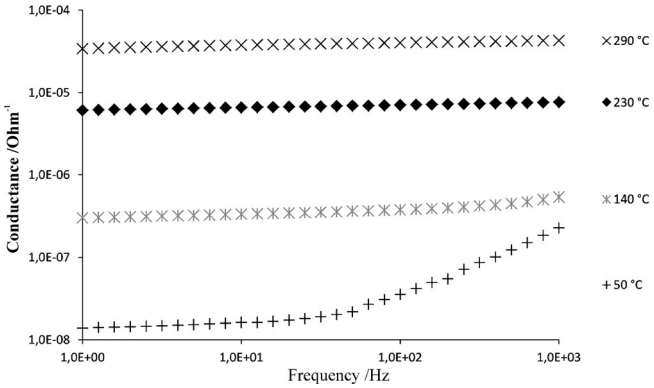

Figure 7. Frequency dependent total conductivity for $Li_{17}Sb_{13}S_{28}$ at different temperatures.

ting these data consists of two series-connected R-CPE elements. During the fit, the exponent variable α of the low-frequency CPE element was fixed at $\alpha = 0.5$ to symbolize Warburg diffusion.

Raman spectroscopy

Raman spectroscopy is well-suited for investigating different building units in crystalline and amorphous compounds. Based on the position and splitting of the Sb–S stretching bands the surrounding of SbS_x units can be implied.[8,24,39,40] Typically Sb–S stretching modes of SbS_3 units are located between 330 and 360 cm^{-1}.[37] However, so-called secondary bonds cause a redshift of these bands. A lowering of the point symmetry of SbS_3 units leads to a splitting of the stretching bands. In the case of the title compound the Raman measurements were performed on powdered samples in sealed Duran glass capillaries. The strong Sb–S stretching modes of the [SbS_5E] units are dominating the Raman spectra. The corresponding bands are located at 315 and 341 cm^{-1}. The redshift results from secondary bonds and corner and edge sharing of the [SbS_5E] units. The weak bands at 156 and 171 cm^{-1} are tentatively assigned to lattice vibrations. The Raman spectrum is shown in Figure 8.

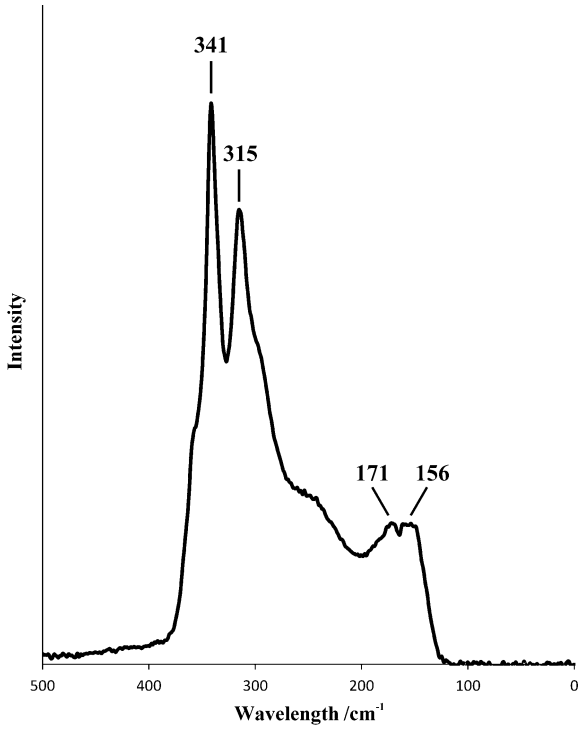

Figure 8. Raman spectrum of $Li_{17}Sb_{13}S_{28}$. The spectrum is dominated by the strong Sb–S stretching modes at frequencies > 300 cm^{-1}.

Thermal analysis (DTA)

DTA measurements were performed on pure powdered samples of $Li_{17}Sb_{13}S_{28}$ sealed in silica ampoules under vacuum. Therefore two heating/cooling cycles in the temperature range from ambient temperature to 1023 K were measured with a rate of 5 K min^{-1}. $Li_{17}Sb_{13}S_{28}$ shows peritectic decomposition at 854 K. At this temperature $Li_{17}Sb_{13}S_{28}$ decomposes into a melt and cubic γ-$LiSbS_2$. At 923 K the liquidus curve is crossed (onset temperatures). Both cycles are identical. This

finding fits well with the phase diagram of Olivier-Fourcade et al.[1]

Conclusion

$Li_{17}Sb_{13}S_{28}$ is a new compound in the quasi binary system Li_2S–Sb_2S_3. It crystallizes in the monoclinic space group *C*2/*m* (no. 12). The powder diffraction pattern of the phase pure product fits very well with that of "$Li_6Sb_4S_9$". Because no further data are available for "$Li_6Sb_4S_9$", it is very likely identical with $Li_{17}Sb_{13}S_{28}$. Impedance spectroscopic measurements show an enhanced ionic conductivity in the range of $2.9\times10^{-9}\ \Omega^{-1}\,cm^{-1}$ at 322 K to $8.0\times10^{-6}\ \Omega^{-1}\,cm^{-1}$ at 564 K. The corresponding Arrhenius diagram provides an activation energy of $E_A = 0.4$ eV below 403 K and of $E_A = 0.6$ eV above. The Raman spectra of $Li_{17}Sb_{13}S_{28}$ show strong Sb–S stretching modes of the $[SbS_5]$ units at 315 and 341 cm^{-1}. In addition, the influence of secondary bonds and corner and edge connections of the $[SbS_5]$ units can be derived from the redshift of the Sb–S stretching modes compared with typically Sb–S stretching frequencies of $[SbS_3]$ units between 330 and 360 cm^{-1}.[8,24,37,39,40] DTA measurements show peritectic decomposition at 854 K into a melt and cubic $LiSbS_2$.

Experimental Section

Synthesis

$Li_{17}Sb_{13}S_{28}$ was synthesized by reaction of Li_2S (99.9%, Alfa Aesar) and Sb_2S_3 (Merck) in the ratio 1.31:1.00. All manipulations were performed in a glove box under argon atmosphere. The reagents were sealed in graphitized, evacuated silica ampoules and annealed for five weeks at 773 K. Dark-red single crystals of $Li_{17}Sb_{13}S_{28}$ could be separated from the reaction product. The product is air and moisture sensitive.

X-ray crystallography

Single crystals of $Li_{17}Sb_{13}S_{28}$ were mounted on an Agilent SuperNova single crystal diffractometer providing monochromatic $Mo_{K\alpha}$ radiation ($\lambda = 0.71073$ Å) at 123 K. Absorption was corrected by multi-scan.[42] The crystal structure was solved by Direct Methods (SIR2004),[41] refined with SHELX-2014,[47] and the positions of the Li atoms were located from difference Fourier maps. All atoms except the split Sb site were refined by using anisotropic displacement parameters. The Sb content on the mixed Li/Sb site was fixed to 25% in the last refinement stages to ensure electric neutrality. Tests for lower symmetry were carried out and did not resolve the antimony split position. Crystallographic data are collected in Table 1.

Powder X-ray diffraction

X-ray diffraction measurements were carried out with a STOE Stadi P diffractometer with monochromatic $Cu_{K\alpha1}$ radiation ($\lambda =$ 1.540598 Å, Ge-monochromator). The powdered samples were measured in sealed glass capillaries ($\varnothing = 0.3$ mm) at room temperature in a 2Θ range from 8 to 90°. Diffraction data were analyzed with WINXPOW.[43]

Impedance spectroscopy

The powdered samples of $Li_{17}Sb_{13}S_{28}$ were cold pressed into pellets with 6000 kg/cm^2. A density of 85% of the calculated density was achieved. Impedance spectroscopic investigations were performed on an IM6d impedance analyzer (Zahner Elektrik). The samples were added to a spring-loaded cell between ion blocking gold electrodes and measured in the frequency range from 1 Hz to 1 MHz and in the temperature range from 323 to 573 K. The data were analyzed with the software Thales Flink.[44] Details of the experimental setup are given elsewhere.[45]

Raman spectroscopy

Raman measurements were performed with a Varian Fourier transform Raman module coupled to a Varian FTS 7000e spectrometer with a Nd:YAG laser with an excitation wavelength of 1064 nm. A liquid-nitrogen-cooled germanium detector was used in backscattering mode. The samples of $Li_{17}Sb_{13}S_{28}$ were powdered and sealed in Duran glass capillaries for the measurements. The resolution was 2 cm^{-1} and the spectra were processed with the Varian Resolution Pro software.[46]

Thermal analysis

DTA measurements were carried out with a Setaram DTA-TG 92–16.18. The powdered samples were sealed in silica capillaries under vacuum. The thermal behavior was investigated in two cycles from room temperature to 1023 K and back with a heating/cooling rate of 5 K min^{-1}. Al_2O_3 was used as external standard.

Acknowledgements

The experimental help of C. De Giorgi, M. Bielmeier, and R. Oppacher is gratefully acknowledged.

Keywords: antimony · ion conductor · lithium · sulfide · thiometalate

[1] J. Olivier-Fourcade, L. Izghouti, M. Maurin, E. Philippot, *Rev. Chim. Miner.* **1983**, *20*, 186.
[2] J. Olivier-Fourcade, M. Maurin, E. Philippot, *Rev. Chim. Miner.* **1983**, *20*, 196.
[3] N. V. Arkhipova, L. D. Leont'eva, A. M. Mikhailova, *Russ. J. Electrochem.* **2003**, *39*, 528.
[4] Z. Nagamedianova, E. Sánchez, *Solid State Ionics* **2006**, *177*, 3259.
[5] Z. Nagamedianova, A. Hernández, E. Sánchez, *Ionics* **2006**, *12*, 315.
[6] Z. Nagamedianova, E. Sánchez, *J. Mater. Sci. Mater. Electron.* **2007**, *18*, 547.
[7] S. Huber, A. Pfitzner, *Z. Anorg. Allg. Chem.* **2014**, *640*, 1596.
[8] S. Huber, C. Preitschaft, R. Weihrich, A. Pfitzner, *Z. Anorg. Allg. Chem.* **2012**, *638*, 2542.
[9] C. Pompe, A. Pfitzner, *Z. Anorg. Allg. Chem.* **2013**, *639*, 296.
[10] H. Sommer, R. Hoppe, *Z. Anorg. Allg. Chem.* **1977**, *430*, 199.
[11] C. Pompe, A. Pfitzner, *Z. Anorg. Allg. Chem.* **2012**, *638*, 2158.
[12] W. Bronger, A. Donike, D. Schmitz, *Z. Anorg. Allg. Chem.* **1999**, *625*, 435.
[13] A. Pfitzner, *Z. Anorg. Allg. Chem.* **1994**, *620*, 1992.
[14] A. Pfitzner, *Z. Kristallogr.* **1998**, *213*, 228.
[15] S. Karup-Møller, E. Makovicky, *Am. Mineral.* **1974**, *59*, 889.
[16] B. J. Skinner, F. D. Luce, E. Makovicky, *Econ. Geol.* **1972**, *67*, 924.
[17] A. Pfitzner, *Z. Anorg. Allg. Chem.* **1995**, *621*, 685.
[18] D. Harker, *J. Chem. Phys.* **1936**, *4*, 381.
[19] E. J. Skoug, J. D. Cain, D. T. Morelli, *Appl. Phys. Lett.* **2010**, *96*, 181905.
[20] M. Kirkham, P. Majsztrik, E. Skoug, D. Morelli, H. Wang, W. D. Porter, E. A. Payzant, E. Lara-Curzio, *J. Mater. Res.* **2011**, *26*, 2001.

[21] N. F. Lugakov, A. S. Lyashevich, E. A. Movchanskii, I. I. Pokrovskii, E. E. Shimanovich, *Dokl. Akad. Nauk BSSR* **1974**, *18*, 825.
[22] K. A. Schönau, S. A. T. Redfern, *J. Appl. Phys.* **2002**, *92*, 7415.
[23] M. Leitl, *Dissertation*, University of Regensburg (Germany), **2007**.
[24] A. Pfitzner, *Chem. Eur. J.* **1997**, *3*, 2032.
[25] T. J. Bastow, H. J. Whitfield, *J. Solid State Chem.* **1981**, *40*, 203.
[26] T. Nilges, *Dissertation*, Siegen (Germany), **2000**.
[27] T. Nilges, S. Reiser, J. H. Hong, E. Gaudin, A. Pfitzner, *Phys. Chem. Chem. Phys.* **2002**, *4*, 5888.
[28] A. Kyono, M. Kimata, M. Matsuhisa, Y. Miyashita, K. Okamoto, *Phys. Chem. Miner.* **2002**, *29*, 254.
[29] H.-H. Nahm, Y.-S. Kim, *Appl. Phys. Lett.* **2013**, *102*, 152101.
[30] L. F. Lundegaard, R. Miletich, T. Balic-Zunic, E. Makovicky, *Phys. Chem. Miner.* **2003**, *30*, 463.
[31] L. F. Lundegaard, E. Makovicky, T. Boffa-Ballaran, T. Balic-Zunic, *Phys. Chem. Miner.* **2005**, *32*, 578.
[32] Z. Mayerová, M. Johnsson, S. Lidin, *Solid State Sci.* **2006**, *8*, 849.
[33] Z. Mayerová, M. Johnsson, S. Lidin, *Angew. Chem. Int. Ed.* **2006**, *45*, 5602; *Angew. Chem.* **2006**, *118*, 5730.
[34] Z. Mayerová, M. Johnsson, S. Lidin, *J. Solid State Chem.* **2005**, *178*, 3471.
[35] W. Hofmann, *Z. Kristallogr., Kristallgeom., Kristallphys., Kristallchem.* **1932**, *84*, 177.
[36] J. Galy, G. Meunier, S. Andersson, A. Åström, *J. Solid State Chem.* **1975**, *13*, 142.
[37] A. Pfitzner, D. Kurowski, *Z. Kristallogr.* **2000**, *215*, 373.
[38] A. Khorassani, A. R. West, *Solid State Ionics* **1982**, *7*, 1.
[39] V. Spetzler, C. Näther, W. Bensch, *Inorg. Chem.* **2005**, *44*, 5805.
[40] R. Kiebach, R. Warratz, C. Näther, W. Bensch, *Z. Anorg. Allg. Chem.* **2009**, *635*, 988.
[41] M. C. Burla, R. Caliandro, M. Camalli, B. Carrozzini, G. L. Cascarano, L. De Caro, C. Giacovazzo, G. Polidori, R. Spagna, *J. Appl. Crystallogr.* **2005**, *38*, 381.
[42] SCALE3 ABSPACK, *CrysAlis RED* software, Version 171.36.28; Oxford Diffraction Ltd: Oxford, UK, **2006**.
[43] STOE, *WinXPOW*, Version 1.08, STOE & Cie GmbH, Darmstadt, **2000**.
[44] *Thales Flink*, Version 2.13; Zahner Messtechnik GmbH & Co. KG, Kronach.
[45] E. Freudenthaler, A. Pfitzner, *Solid State Ionics* **1997**, *101–103*, 1053.
[46] *Resolutions Pro Software*, Molecular Spectroscopy Solutions, Varian Inc., Version 4.1.0.101, **2006**.
[47] G. M. Sheldrick, *Acta Crystallogr. Sect. C* **2015**, *71*, 3.
[48] R. D. Shannon, *Acta Crystallogr. Sect. A* **1976**, *32*, 751.
[49] A. Puls, C. Näther, R. Kiebach, W. Bensch, *Solid State Sci.* **2006**, *8*, 1085.

Received: May 26, 2015
Published online on August 11, 2015